Journal of Geophysical Research: Space Physics

Supporting Information for

On the dynamics of ultra-relativistic electrons (>2 MeV) near L* = 3.5 during 8 June 2015

Benjamin Hogan[1,2], Xinlin Li[1,2], Zheng Xiang[3], Hong Zhao[4], Yang Mei[1,2], Declan O'Brien[1,2], Daniel N. Baker[1,2], Shrikanth Kanekal[5]

[1]Laboratory for Atmospheric and Space Physics, University of Colorado Boulder, Boulder, CO, USA, [2]Department of Aerospace Engineering Sciences, University of Colorado Boulder, Boulder, CO, USA, [3]Department of Space Physics, School of Electronic Information, Wuhan University, Wuhan, China [4]Department of Physics, Auburn University, Auburn, AL, USA, [5]NASA Goddard Space Flight Center, Greenbelt, MD, USA

Corresponding author: Benjamin Hogan (ben.hogan@lasp.colorado.edu).

Contents of this file

Figure S1: 7-9 June 2015 phase space density profiles from Van Allen Probe B

Figure S2: 7-9 June 2015 phase space density at L* = 3.5 from both Probes

Figure S3: Local number density and plasmapause crossings during 7-8 June 2015

Figure S4: Time-averaged wave power spectral density near 4:45 UT 8 June 2015 and Gaussian fit

Figure S5: Dispersion relationship results and resonant energy regions for representative He+ and O+ band EMIC waves

Figure S6: Energy and cross diffusion terms for both He+ and O+ band EMIC waves

Figure S7: Observed and simulated PSD at μ = 1500, 2000, 2500, and 3000 MeV/G

Figure S8: Partial ion composition and lack of oxygen torus presence

Figure S1: 7-9 June 2015 phase space density profiles from Van Allen Probe B

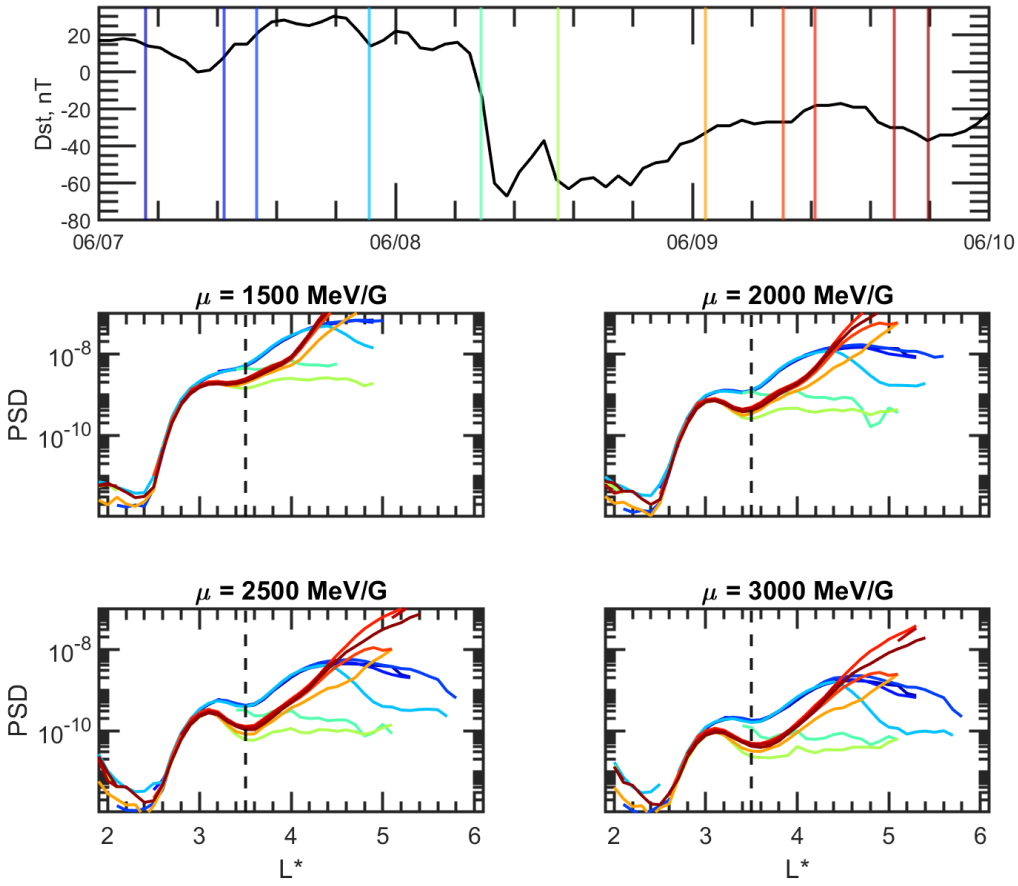

We focus on results from Van Allen Probe A data in the main text. Here, we present radial profiles of phase space density (PSD) for the same adiabatic invariant values and period as shown in Figure 1 of the main text, however, for Probe B. K = 0.10 $G^{1/2}R_E$ and L* bins are 0.1 wide, and adiabatic coordinates are found as calculated using the TS04D magnetic field model, as in Figure 1. We note that similar observations are made from the Probe B data, a local minimum that develops near L* = 3.5 for multi-MeV electron PSD. We note that Probe A observed during one satellite pass near the storm main phase a local extremum at L* = 4.5 that we proposed is an adiabatic effect and function of the local magnetic field not being accurately represented at high L* during the main phase of the storm. This effect is not shown here in the Probe B data, which substantiates that claim. Probe B makes one satellite observation of L* = 3.5, K = 0.10 $G^{1/2}R_E$ just as the decrease in Dst occurs. Therefore, the magnetic field model is also unlikely to perfectly represent the actual magnetic configuration during this time, which may contribute to the transitional measurement made by Probe B here during the satellite pass at ~6 UT 8 June 2015 which is denoted by a green line. The PSD profile at this time shows an intermediate measurement between the pre-storm PSD and the post-storm local minimum that develops at L* = 3.5.

Figure S2: 7-9 June 2015 phase space density at L* = 3.5 from both Probes

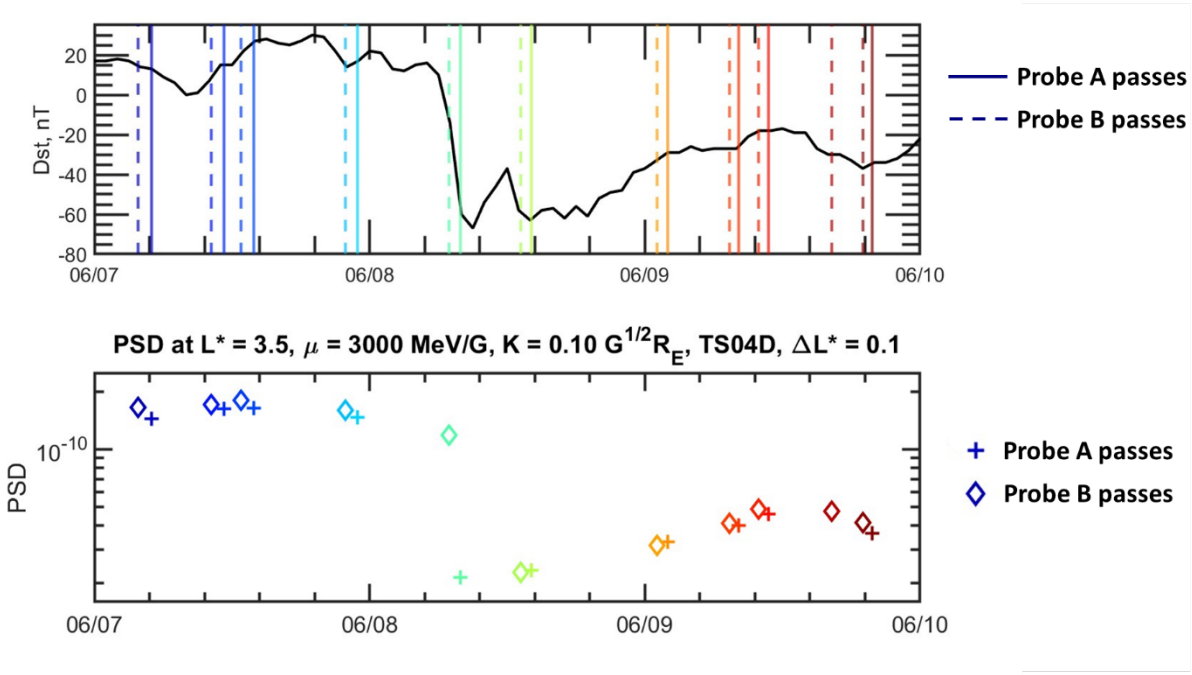

To compare the PSD specifically at L* = 3.5 during the event, and to compare the observations from Probe A and B, we show the PSD from each Probe at L* = 3.5 in Figure S2. The top panel shows the Dst for 7 through 9 June 2015, and vertical colored lines indicate passes by each Probe which observe multi-MeV electrons at L* = 3.5, K = 0.10 $G^{1/2}R_E$. Solid vertical lines indicate passes by Probe A, dashed vertical lines indicate passes by Probe B. In the bottom panel is the calculated PSD at μ = 3000 MeV/G, the highest energy population shown in the main text for which the local minimum in PSD develops. Diamonds indicate PSD calculated from Probe A measurements, and + marks indicate those from Probe B. Here we see the rapid decrease in PSD as seen by both Probes in the first half of 8 June 2015. However, Probe B maintains higher measurement of PSD for one more satellite pass than Probe A. The passes where Probe B maintains higher measurement near 6 UT 8 June 2015 and Probe A subsequently shows large decrease are indicated in green and are near the main phase of the storm. It is possible that during this rapid decrease in PSD, the magnetic field model is not accurately representing the real dynamics of Earth's magnetic field during this time, and that is contributing to a large perceived difference in the measurements from Probe A and B, which here occur within 1.1 hours. It is unlikely that the loss observed will occur within this 1.1-hour period alone, but possible over one satellite orbit. In subsequent data from the second half of 8 June 2015 and on, both Probes have similar PSD measurements.

Figure S3: Local number density and plasmapause crossings during 7-8 June 2015

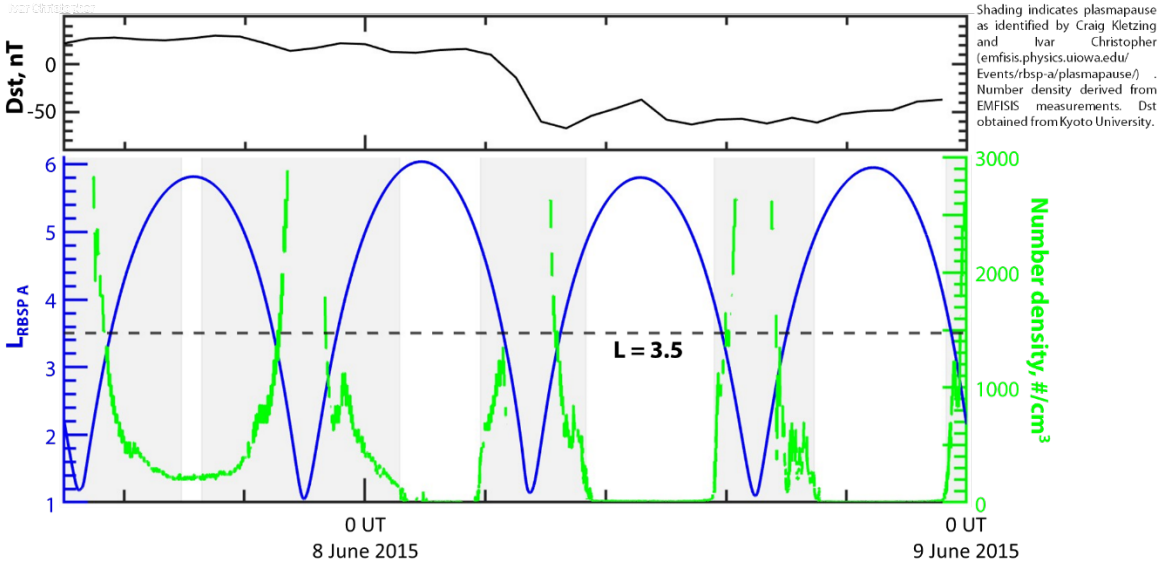

The local number density is important in this study as it affects the solution of the plasma dispersion relation and indicates which density region the spacecraft is in, relative to the plasmapause. In Figure S3 we show the Dst, and the number density as derived from EMFISIS data, and L value of the spacecraft for 12 UT 7 June – 0 UT 9 June 2015. Analysis of the local number density by EMFISIS PI Craig Kletzing has been conducted and the plasmapause crossings by the spacecraft are reported using this data. Using this information, we here shade regions where the spacecraft is within the plasmapause. A dashed horizontal line is shown at L = 3.5, near the region of PSD loss discussed in the manuscript. This shows that this region L = 3.5 is well within the plasmapause. Further inspection of the actual number density, shown in green on the right y axis, indicates local number density near and greater than ~1000 /cm^3, which indicates a dense and likely cold plasma region. Therefore, the observed loss feature occurs within the plasmapause, and a cold plasma dispersion relation as approximated in the manuscript is appropriate for modeling waves in the local medium.

Figure S4: Time-averaged wave power spectral density near 4:45 UT 8 June 2015 and Gaussian fit

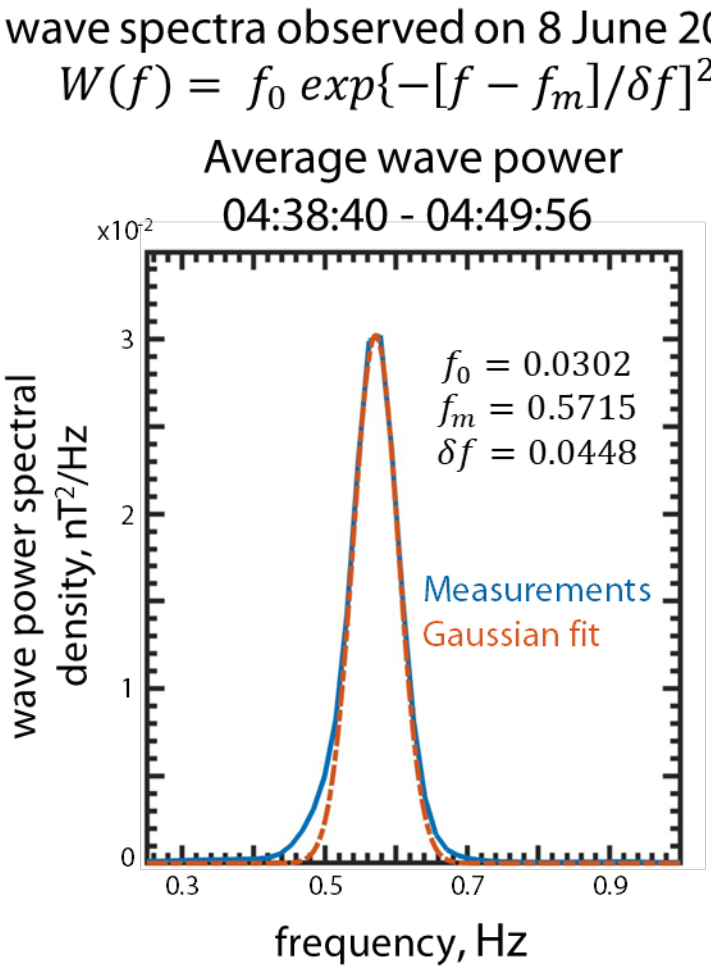

Figure 3 in the manuscript shows the wave power spectral density from 0 – 6 UT 8 June 2015. In Figure 3 we identified regions of EMIC power, including one region near 04:38:40 - 04:49:56 UT. Here, we time-average this wave power spectral density. This average power during this period is shown in blue in Figure S4. A Gaussian fit in red is prescribed to this peak, and matches the observations well.

Figure S5: Dispersion relationship results and resonant energy regions for representative He+ and O+ band EMIC waves

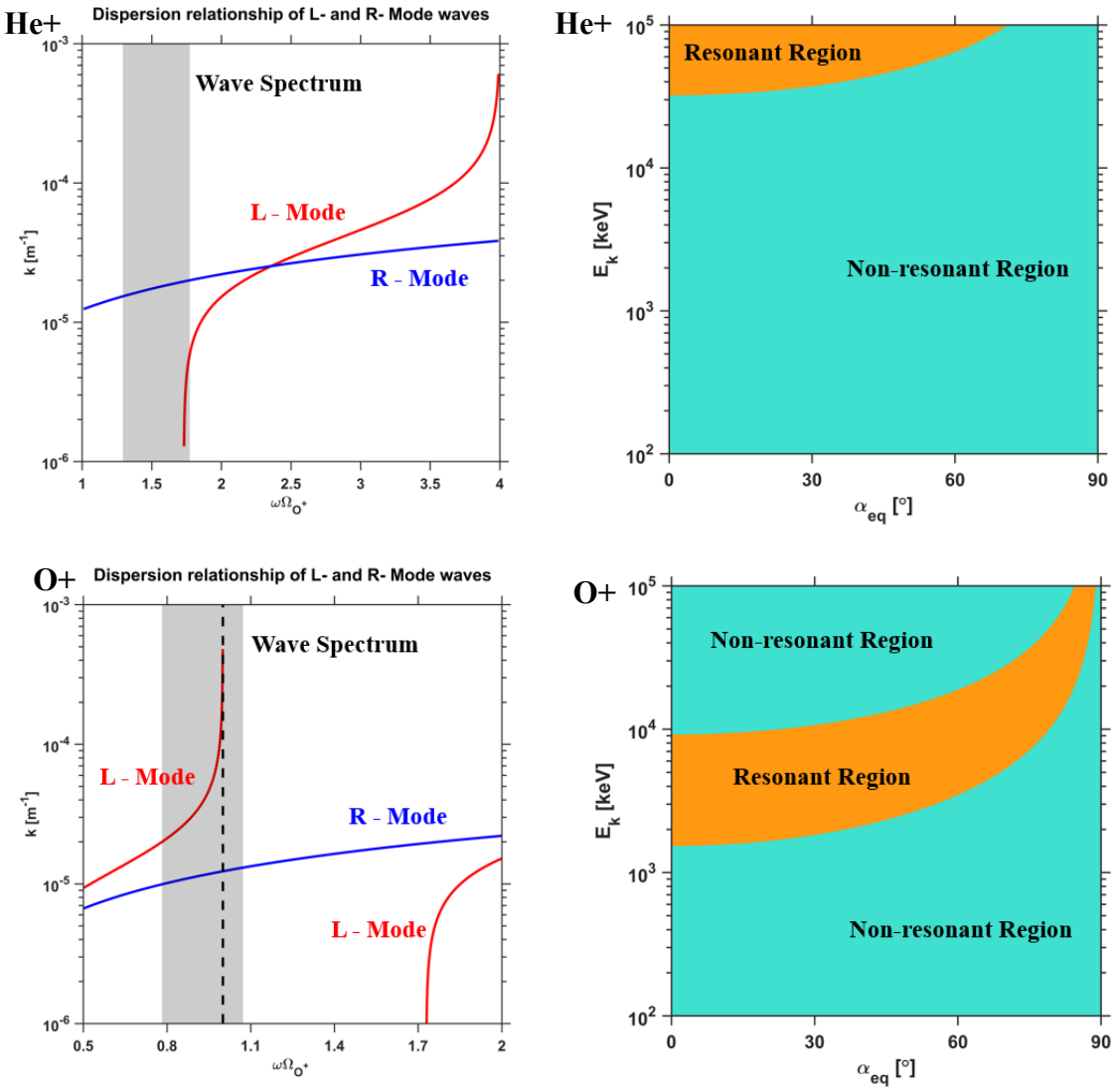

In this study we solve the cold plasma dispersion relation (e.g., Summer et al., 2007) by use of the Full Diffusion Code (Ni et al., 2008, 2011; Shprits and Ni et al., 2009). Here, we show results for the solution of the wave number k, as a function of frequency normalized to the oxygen gyrofrequency ω/Ω_{O+} for both cases considered in the paper. These two cases are, H+ band EMIC waves, and O+ band EMIC waves. The results of the dispersion relation are shown in the left panels for each of these two cases; The solution He+ band waves are shown in the top left panel, the solution for O+ band waves is shown in the bottom left panel. Both the L and R modes are shown here for completeness, while we consider only L-mode waves in this study due to their high occurrence rate from studies of EMIC waves during the Van Allen Probes era, discussed in the main text. The wave spectrum indicated on each plot is the width of the EMIC wave spectra observed just before the satellite crossing of L* = 3.5, in the He+ case this has been scaled according to the local magnetic field, in the O+ case, we maintain the frequency spectrum. Because this then

shifts the spectra to frequencies greater than the O+ frequency, we then limit the actual wave spectra to 0.99 times the local O+ gyrofrequency.

On the right are the explicit resonant regions for each of the two wave types. Minimum resonant energies of electron with EMIC waves are discussed in the main text (see equation 2). For a full discussion of minimum resonant energies, we refer the reader to Summers et al., (2003). The resonant region for He+ band waves is shown in the top right, and shows minimum resonant energies of 32 MeV at 0 degree pitch angles and 56 MeV at 54 degree pitch angles (which corresponds to $K = 0.10\ G^{1/2}R_E$) much higher than the energies of the observed loss feature discussed in this study. In the bottom right we show the explicit resonant region for O+ band EMIC waves, which here has minimum resonant energies of 1.4 MeV at 0 degree pitch angle, and 2.8 MeV at 54 degrees pitch angle. Thus, O+ band EMIC waves could be contributing to the loss of multi-MeV electrons, He+ band waves resonate here only with electron energies much higher than those observed to be lost during the event of study.

Figure S6: Energy and cross diffusion terms for both He+ and O+ band EMIC waves

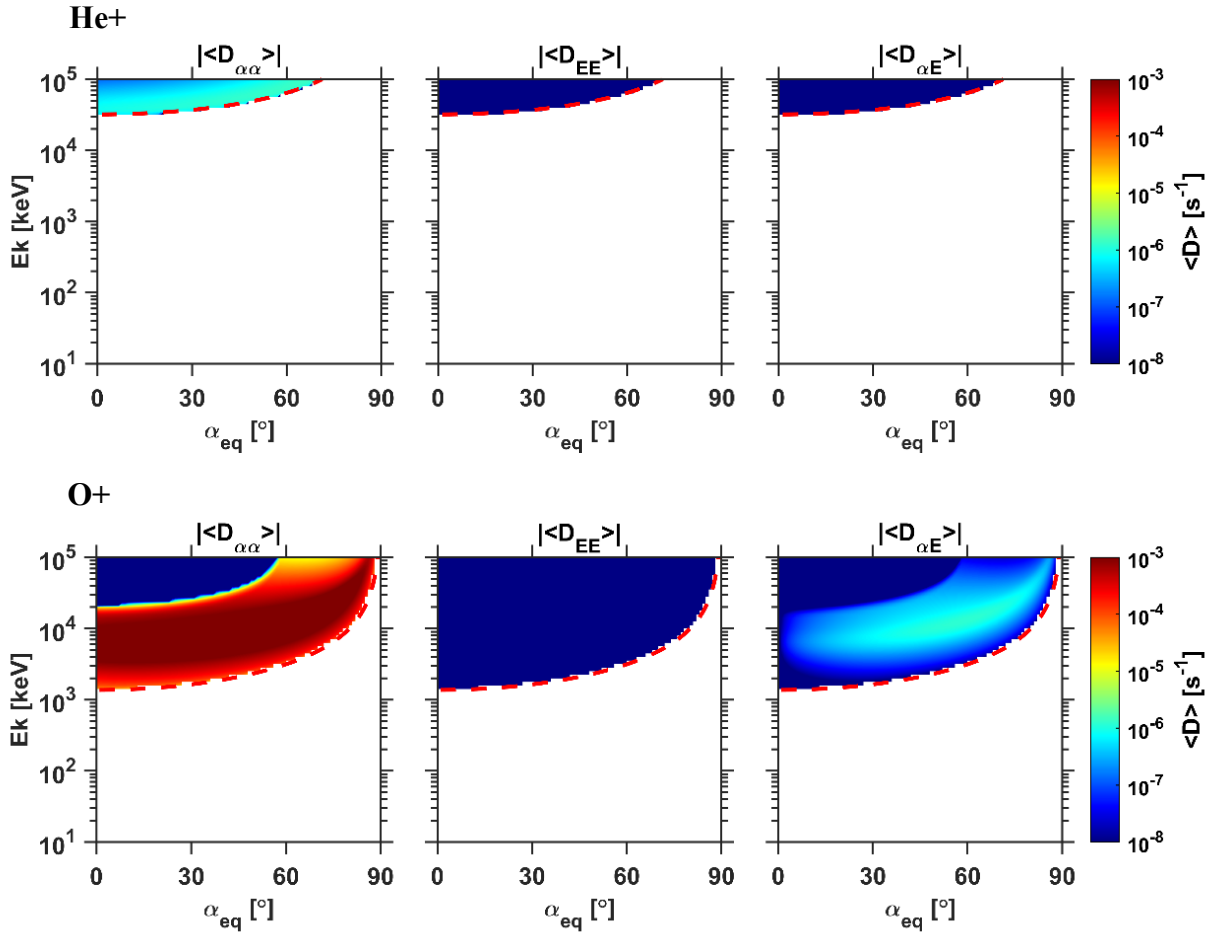

In this study we here consider only the effects of pitch angle scattering due to EMIC waves. EMIC waves can also cause energy diffusion and cross diffusion of trapped particles, the explicit equations for each of these diffusion coefficients is discussed in Summers et al., (2007). Here, we use the Full Diffusion Code (Ni et al., 2008, 2011; Shprits and Ni et al., 2009) to calculate these parameters. We compare the pitch angle diffusion coefficient $D_{\alpha\alpha}$ is with the energy diffusion coefficient D_{EE} and the cross diffusion coefficient $D_{\alpha\mathrm{E}}$ in Figure S6 for both He+ and O+ band EMIC wave cases discussed in the main text. When comparing the diffusion coefficients due to O+ band EMIC waves (bottom row), it is shown that D_{EE} is ~5 orders of magnitude less than $D_{\alpha\alpha}$ for the energies of interest, and $D_{\alpha\mathrm{E}}$ is about 3 orders of magnitude less than $D_{\alpha\alpha}$. Therefore, these other diffusion mechanisms are minor compared to the effects of pitch angle scattering here, and negligible. Thus, the pure-pitch angle diffusion model used here for PSD evolution is sufficient for modeling major effects of EMIC waves on the populations of study.

Figure S7: Observed and simulated PSD at μ = 1500, 2000, 2500, and 3000 MeV/G

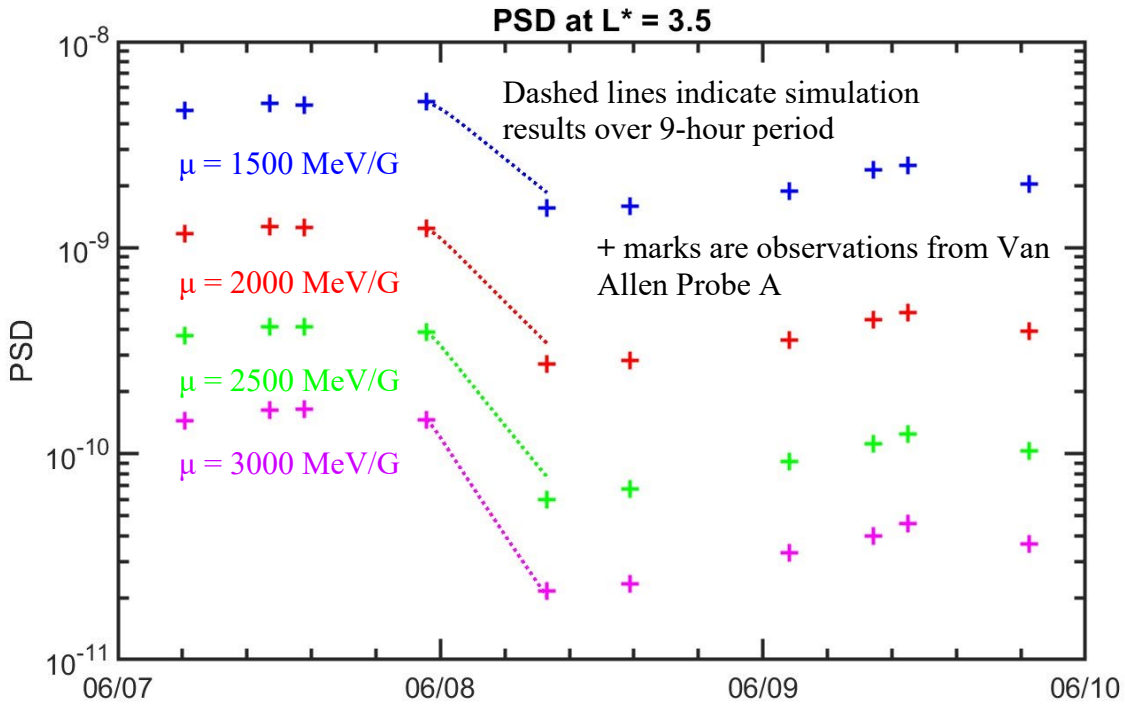

Figure 5 in the main text describes in detail the simulation result of PSD as a function of pitch angle for μ = 3000 MeV/G electrons, and compares the simulation results to observations from Van Allen Probe A. Here we show results for the complete set of diagnostic μ values discussed in this study, 1500, 2000, 2500, and 3000 MeV/G. These values correspond to 3.4, 4, 4.5, and 5.0 MeV electrons, respectively, at $K = 0.10\ G^{1/2}R_E$, L* = 3.5, during the event of study when adiabatic coordinates are found with the TS04D magnetic field model. Here, marks indicated by "+" are observations from Van Allen Probe A at L* = 3.5, $K = 0.10\ G^{1/2}R_E$ for the period 7 through 9 June 2015. Observations color coded to the μ labels on the plot.

PSD is simulated by prescribing initial PSD spectra and matching the PSD at 54° equatorial pitch angle to the observations (54° corresponds to $K = 0.10\ G^{1/2}R_E$). The PSD is then simulated for 9 hours, the period during which rapid loss is observed here by Van Allen Probe A. The dashed lines represent the PSD simulation result, evaluated at 54°, over the 9 hour period simulated. These results show decrease from each energy comparable to the observations.

Figure S8: Partial ion composition and lack of oxygen torus presence

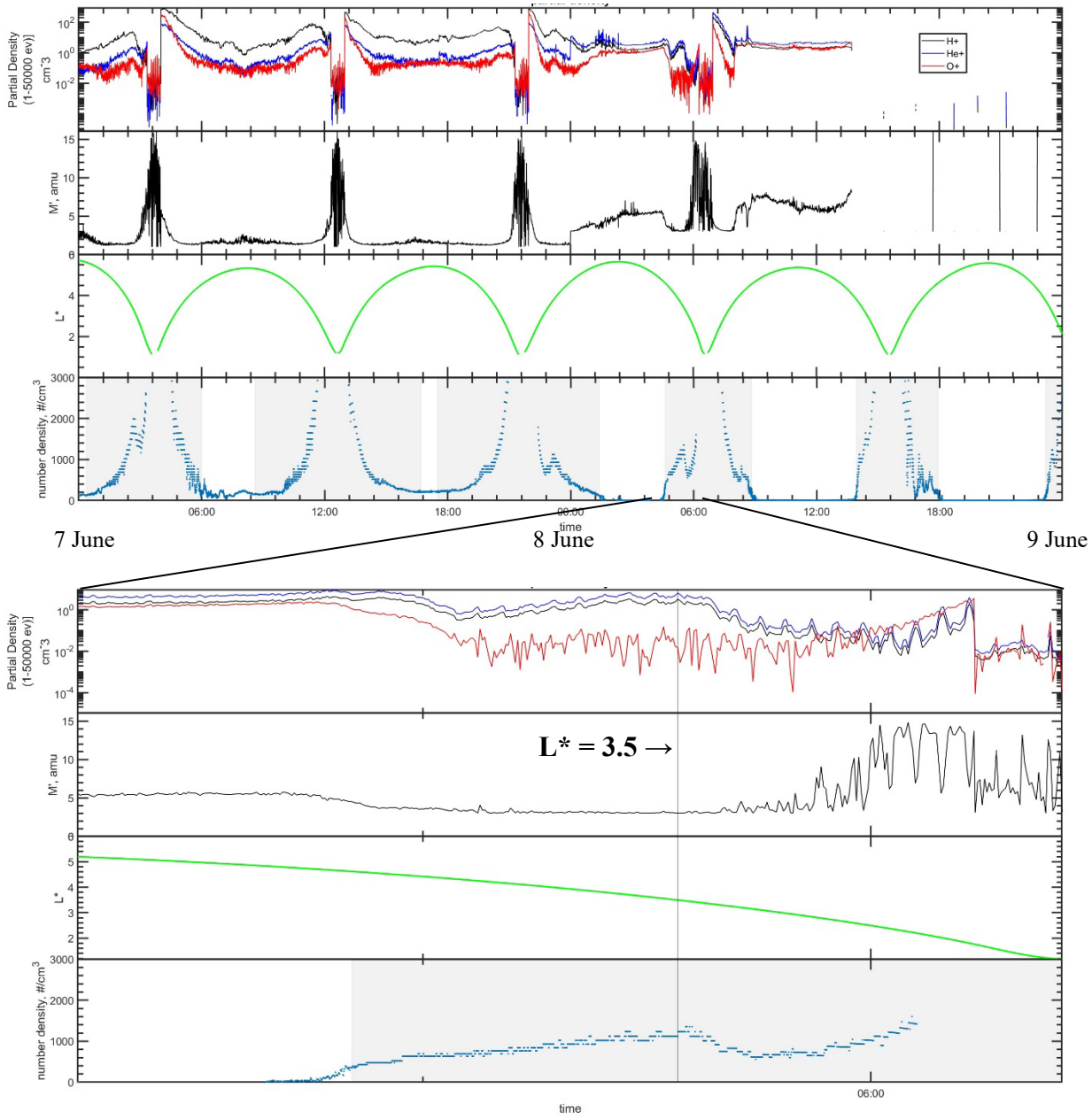

Studies by Yu et al., (2015) suggest that many O+ band EMIC waves are correlated with the oxygen torus (Nose et al., 2015), a region of dense oxygen that forms near the outer edge of the plasmasphere during certain periods. Nose et al., (2015) have studied HOPE data and used the methods of Goldstein et al., (2014) for calculating partial densities of ions for >eV energies (lower than the standard HOPE data product considers for ion densities). Nose et al., (2015) introduce the parameter M', the average mass density of the local plasma from the major species H+, He+, and O+, as found from this ion composition calculation from HOPE. Here, we calculate the partial ion densities and M' as described by Goldstein et al., (2014) and Nose et al., (2015) respectively, using data from Van Allen Probe A. The top panel of the first figure shown above is the partial ion

composition. The second panel is M'. The third panel is the L* of the spacecraft corresponding to $K = 0.10\ G^{1/2}R_E$, and the fourth panel is the local number density as found from analysis of EM-FISIS data. Shaded regions in the fourth panel indicate regions when the spacecraft is within the plasmapause, described prior. We show in the first figure this data for 7 through 9 June 2015 to show parameters before and after the event. HOPE data is unavailable for the second half of 8 June 2015.

In the lower figure, we show these same parameters, focused on the first inbound pass of the spacecraft on 8 June 2015 during which rapid PSD loss is observed. During this pass, there is no appreciable increase in M', or the O+ partial ion composition near L* = 3.5. Rather, M' does not increase until much lower, at L* < 3. Therefore, we do not find evidence of the oxygen torus at L* = 3.5 during this event.